Energy 286 (2024) 129629

Contents lists available at ScienceDirect

Energy

journal homepage: www.elsevier.com/locate/energy

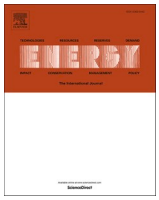

Investigation on recirculated regenerative solid desiccant-assisted dehumidification system: Impact of system configurations and desiccant materials

Minqi Su [a,b], Xiaoqu Han [a,*], Yanbing Dai [a], Jinshi Wang [a], Jiping Liu [b], Junjie Yan [a]

[a] State Key Laboratory of Multiphase Flow in Power Engineering, Xi'an Jiaotong University, Xi'an, 710049, China
[b] MOE Key Laboratory of Thermal Fluid Science and Engineering, Xi'an Jiaotong University, Xi'an, 710049, China

ARTICLE INFO

Keywords:
Desiccant wheel
Recirculated system
Dehumidification
Desiccant material

ABSTRACT

Desiccant wheels (DWs) have emerged as highly promising alternatives for achieving efficient dehumidification, low-carbon and energy-saving initiatives. The present work aimed to determine the optimal system configuration for dehumidifying enclosed spaces using a DW-based system with the recirculated regeneration of process air based on modelling investigation, which has been validated with experiments. Three distinct configurations of this DW-based system were compared. The impact of operational parameters and desiccant materials on the system dehumidification capacity (D_{tot}) and energy efficiency was thoroughly analyzed. The results indicate that the posterior diversion of regeneration air was most preferable for improved dehumidification performance, enhancing the D_{tot} and the improvement of moisture removal capacity (ΔMRC) by 3.7 % and 42.8 %, respectively. Moreover, posterior diversion emerged as a compelling option for energy conservation as it reduced the energy consumption by 13.3 %. Furthermore, six different desiccant materials were compared, and it was found that the synthesized metal silicate material was most suitable for the proposed systems, improving the optimal ΔMRC by 32.2 %. Furthermore, a strong correlation was identified between the maximum adsorption capacity and the proposed system performance. Overall, these findings aid in developing a promising method for enclosed space dehumidification and cooling.

1. Introduction

The realization of high-quality thermal environments by employing low-carbon methodologies has garnered significant interest. The precise control of the temperature and humidity within enclosed spaces, such as diving apparatus and underground shelters, poses unique challenges different from those encountered in conventional residential environments. These specialized spaces are characterized by their fully sealed and airtight designs, which necessitate the careful consideration of various factors for effective temperature and humidity management [1]. Therefore, there exists an urgent need to realize dehumidification in an enclosed space. Nevertheless, the traditional air conditioning systems frequently employed for indoor air quality management are known to consume excessive amounts of energy, particularly in regions with hot and humid climates [2]. Therefore, the adoption of an energy-efficient dehumidification method is of paramount importance.

The desiccant wheel (DW)-based dehumidification system emerges as a superior alternative to traditional vapor compression systems to achieve efficient dehumidification in enclosed spaces. With its ability to harness waste heat and its environmentally friendly nature, the DW-based system aligns with the goals of energy efficiency and sustainability [3]. DW is composed of a dehumidification section and a regeneration section [4]. The moisture from the process air is removed by desiccants via adsorption because of the vapor pressure difference between the desiccants and the air. Then, the desiccants are desorbed in the regeneration section [5]. Therefore, the system dehumidification capacity can be improved by the removal of moisture from unsaturated humid air. A multitude of experimental studies on DWs have been conducted [6]. The desiccant material, which is the most important part of the DW, has been the focus of many studies [7]. Song et al. [8] experimentally analyzed the thermal performance of a phase change material that was used as the desiccant. Su et al. [9] experimentally investigated the enclosed DW dehumidification system and found out that the system dehumidification capacity could be improved using a

* Corresponding author.
E-mail address: hanxiaoqu@mail.xjtu.edu.cn (X. Han).

https://doi.org/10.1016/j.energy.2023.129629
Received 20 June 2023; Received in revised form 13 October 2023; Accepted 8 November 2023
Available online 11 November 2023

desiccant-based system. DW regeneration, which is the crucial process in DW-based dehumidification, has also been studied for a long time [10]. Asadi et al. [11] compared different regeneration configurations to identify the optimum one for a DW- based system. Su et al. [12] optimized the performance of the DW-based system by exergy analysis. Ge et al. [13] compared the exergy efficiency between a DW-assisted dehumidification system and the conventional vapor compression dehumidification system, and they found out that the exergy efficiency of the condensation dehumidification system was 3–4 times higher than that of the DW based system. Numerous findings regarding the optimization of both the DW system and materials utilized in the process have been previously reported, but all these studies had certain limitations in terms of experimental investigations.

Many theoretical studies have been conduted to overcome the limitations of experimental investigations in previous studies [14]. Among the commonly used theoretical methods, numerical modeling [15], machine learning modeling [16], and empirical modeling are widely used for DWs [17]. Physical characteristics are considered in the numerical models, including the gas side resistance (GSR) model and the gas and solid side resistance (GSSR) model [18]. Wang et al. [19] established a control model to determine the optimal working condition of a DW. The artificial neural network (ANN) method was mainly adopted to simulate the DW performance in the machine learning model. The main square error (MSE) of the simulation results was generally low based on the ANN model [20]. Jani et al. [21] theoretically analyzed the thermal and dehumidification performance of the solid desiccant vapor compression system using the ANN method. The maximum percentage difference between the experimental and numerical results was 13.4 %. Motaghian et al. [22] trained different ANN structures to investigate the influence of internal and external parameters on the DW performance, and the MSE of the results was around 5.9×10^{-5}. Sahu et al. [23] applied a radial basis neural network to simulate the performance of a DW. Chen et al. [24] adopted multi regression and the ANN model to analyze the impact of dimensionless parameters on the outlet states of a DW. An empirical model was established through the data processing of the experimental or numerical results [25]. Zendehboudi [26] carried out a genetic algorithm-least square support vector machine model to simulate the performance of a DW. Kang et al. [27] established an analytical model to predict the outlet states of a DW with different area ratios between the process and regeneration sections. Guan et al. [28] investigated the regeneration energy consumption of DW-assisted system employed at the 2022 Winter Olympics using an empirical model. The results reveal that the carbon emission could be reduced by 42 % when low humidity air was used for regeneration. A numerical method is also suitable for the feasibility and economic analysis of the DW system [29].

The DW is commonly used in dehumidification systems due to its ability to continuously perform two key functions: dehumidification and regeneration. However, conventional DW systems are typically open systems, in which a dedicated stream of fresh air is required for the regeneration process [30]. Different configurations have been proposed to attain improved system performance. The Pennington cycle [31], Dunkle cycle [32], and the solid dry cooling circulation cycle [33] are typical open cycles used in desiccant cooling systems. In enclosed spaces, no surplus dry fresh air is available for use as the regeneration air [34]. Therefore, to address the challenge of dehumidification in enclosed spaces, a closed cycle DW-assisted system has emerged as a highly compelling solution.

To the best of the authors' knowledge, the majority of previous studies predominantly focused on open cycle systems, so the significance of closed cycle systems was disregarded. Moreover, the impact of material properties on the system performance has been largely overlooked, and studies have thus mainly focused on the influence of external parameters. In addition, in the prior work of these authors [9], a novel dehumidification system using recirculated regenerative DW was presented for dehumidification in enclosed space, and experimental investigations were conducted to evaluate the system's dehumidification capabilities and its exergy distribution. Nevertheless, the outcomes were predicated upon the particular DW, and only a limited range of operational conditions was considered. Furthermore, the absence of theoretical models impedes the evaluation of the system applicability to different DWs. Finally, no comparative investigation of distinct system configurations has been performed. Therefore, the present work aimed to further optimize the performance of the recirculated regenerative solid desiccant (RRSD) system through theoretical analysis, and investigate the influence of both operational and material parameters. In addition, a sensitivity analysis of crucial material parameters was conducted and a comparison of different recirculation configurations was made to identify the optimal solution of the RRSD system.

2. System description

The focus of the present work was on the analysis and evaluation of the RRSD system. The RRSD system, as illustrated in Fig. 1(a), operates by utilizing the circulating portion of the process air as the regeneration air for DW. The operation of a standard RRSD system begins when hot and humid ambient air undergoes preliminary treatment in a precooler before entering the dehumidification section of the DW. Within this section, the air is subjected to further dehumidification, resulting in the removal of excess moisture. Subsequently, the dry and cold air is divided into two distinct streams. One part is heated to the desired temperature in an air heating device, which then serves as the regeneration air for the DW. The other part of the air enters directly into the condenser, where it undergoes further dehumidification. Subsequently, the two air streams are combined and undergo a final cooling process within the condenser, ensuring optimal temperature and humidity. Finally, the cool and dehumidified air is supplied to the enclosed space, as required.

The RRSD system is distinguished by its ability to redirect a portion of the processed air as regeneration air to the DW. The diversion process, including preliminary diversion that is the most energy-efficient but results in higher humidity of the regeneration air, can be executed under various circumstances. Furthermore, pre-treating the process air before diversion can effectively reduce the humidity of the regeneration air, albeit at the cost of increasing the amount of the precooling air. This can be accomplished by utilizing a configuration similar to those shown in Fig. 1(b) and (c). The process air is divided into two streams before passing through the precooler in Fig. 1(c), while it is divided after passing through the precooler in Fig. 1(b). Notably, this bifurcation enhances the system flexibility, allowing the designer to decrease energy consumption and optimize dehumidification performance by adjusting the flow rate of each air stream, according to the requirements of the specific application.

3. Models and methodology

3.1. Desiccant wheel model

In this work, a mathematical model based on the one-dimensional GSR model was established for the RRSD-assisted dehumidification system [18]. The model was formulated using MATLAB, and the differential equations were discretely solved using the windward difference scheme. The computational flowchart of this approach is depicted in Fig. 2. The simulation process involved the input of the DW properties and the initial conditions. These inputs were carefully integrated to facilitate the calculation of both the process and regeneration cycles. The boundary conditions of regeneration inherent to the analyzed system, are distinct and deviate from those typically employed for open systems. After the diverse system configurations under investigation were identified, appropriate regeneration boundary conditions tailored to each specific setup were carefully selected. The system performance was then evaluated by analyzing the simulation results generated after each 30 min cycle. The model was established on the basis of the

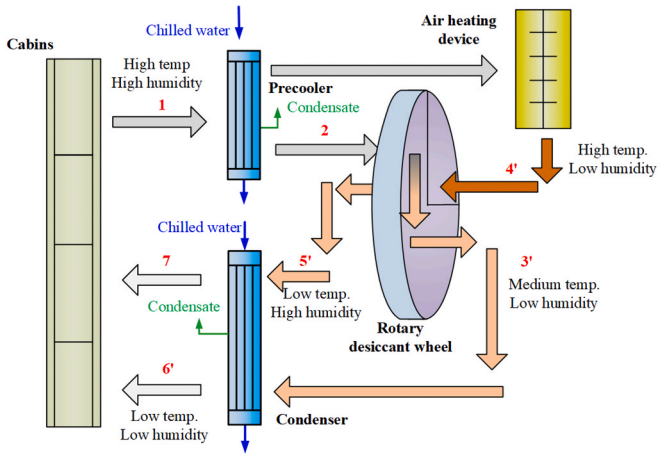

(a) System A

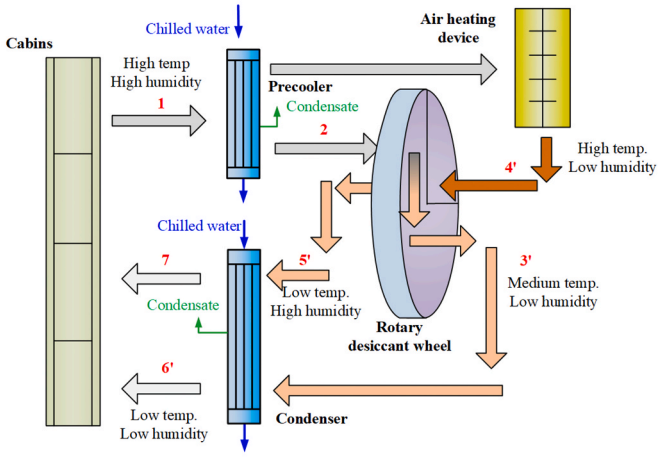

(b) System B

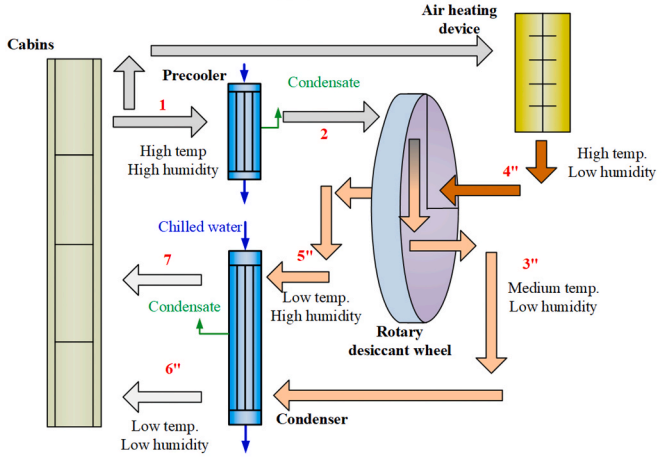

(c) System C

Fig. 1. Working principle of proposed system.

following assumptions:

(1) Solid side resistance in the air was neglected.
(2) The thermodynamic properties of the desiccant, vapor, and air remained constant.
(3) The coefficient of heat and mass transfer between the desiccant wall and air was constant along the air channel.
(4) There was no air leakage.
(5) The material and the air flow rates at the inlet of the DW were kept constant.

3.1.1. Governing equation

The main equations of the DW model are as follows:

The mass conservation equation between the air and desiccant takes the following form:

$$\frac{\partial \omega_a}{\partial \tau} + V\frac{\partial \omega_a}{\partial z} + \frac{f_d}{2A\rho_a}\frac{\partial \omega_d}{\partial \tau} = 0 \tag{1}$$

where ω_a represents the humidity ratio of air, kg·kg^{-1}; ω_d represents the humidity ratio of the air at the surface of the desiccant, kg·kg^{-1}; τ is time, s; V represents the velocity of the air, m·s^{-1}; z represents the axial coordinate, m; A is the cross-section area of channel, m^2; and f_d represents the mass per unit length in a single channel of the desiccant, kg·m^{-1}.

A sketch of the control volume for the model developed is shown in Fig. 3, where L represents the length of the DW, m; and δ represents the half thickness of the desiccant wall, mm.

The mass conservation in the desiccant is derived as:

$$\frac{\partial W}{\partial \tau} + \frac{2K_y P}{f_d}(\omega_d - \omega_a) = 0 \tag{2}$$

where W represents the moisture in the desiccant, kg·kg^{-1}; and P is the perimeter of the desiccant channel, m.

The energy conservation between air and desiccant is calculated as follows:

$$\frac{\partial T_a}{\partial \tau} + V\frac{\partial T_a}{\partial z} + \frac{f_d\left(c_{pd} + Wc_{pl}\right) + f_m c_{pm}}{2A\rho_a\left(c_{pa} + \omega_a c_{pv}\right)}\frac{\partial T_w}{\partial \tau} + \frac{K_y P Q_{st}}{A\rho_a\left(c_{pa} + \omega_a c_{pv}\right)}(\omega_d - \omega_a) = 0 \tag{3}$$

where T_a represents the temperature of air, K; T_w represents the temperature of the desiccant wall, K; c_p represents the specific heat capacity, J·(kg·K)$^{-1}$; and Q_{st} is the adsorption heat of the desiccant material, J·kg^{-1}.

The heat transfer in the desiccant is expressed as follows:

$$\frac{\partial T_w}{\partial \tau} + \frac{2\alpha P}{f_d\left(c_{pd} + Wc_{pl}\right) + f_m c_{pm}}(T_w - T_a) + \frac{2K_y P Q_{st}}{f_d\left(c_{pd} + Wc_{pl}\right) + f_m c_{pm}}(\omega_d - \omega_a) + \frac{2K_y P c_{pv}}{f_d\left(c_{pd} + Wc_{pl}\right) + f_m c_{pm}}(\omega_d - \omega_a)(T_w - T_a) = 0 \tag{4}$$

The supplementary equations of the model are as follows:

The relationship between the humidity ratio and the relative humidity is calculated as follows:

$$\omega = \frac{0.62188\varphi_d}{\frac{P_{atm}}{P_{vs}} - \varphi_d} \tag{5}$$

where P_{atm} is the atmosphere pressure, Pa; P_{vs} represents the vapor saturation pressure, Pa; which can be calculated as follows:

$$P_{vs} = e^{\left(23.196 - \frac{3816.44}{T_w - 46.13}\right)} \tag{6}$$

The sorption isotherm equation is as follows:

$$\varphi_d = \frac{R \times \frac{W}{W_{max}}}{1 + (R-1) \times \frac{W}{W_{max}}} \tag{7}$$

where R represents the separation factor, and W_{max} represents the maximum absorption capacity.

In the proposed system, the Reynolds number in the air flow channels of the DW is less than 2300. This corresponds to a fully developed

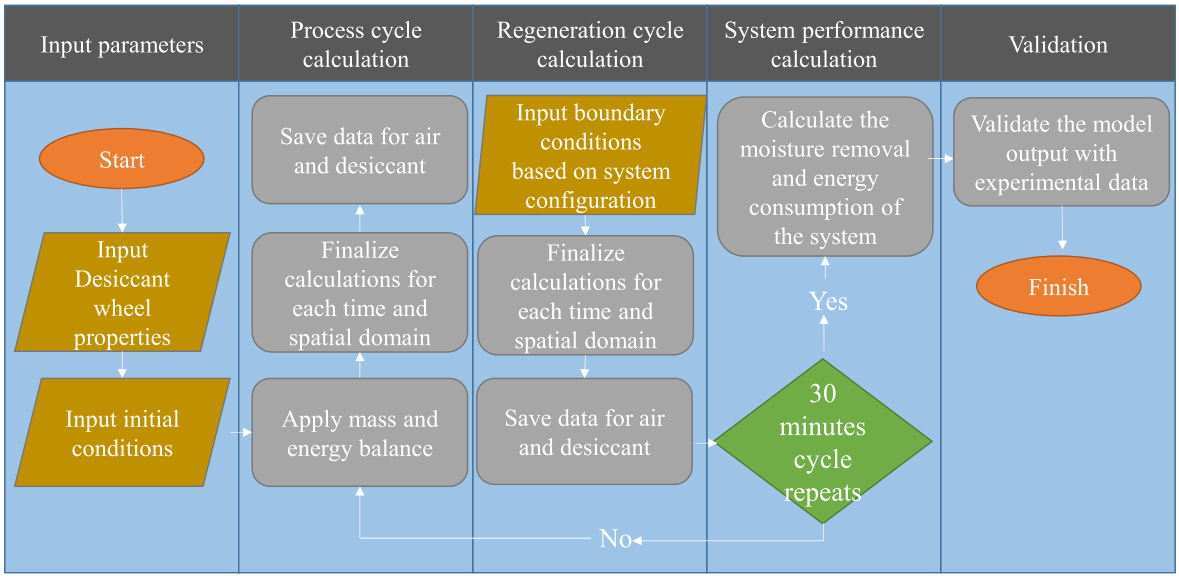

Fig. 2. Calculation flowchart of RRSD system.

laminar flow with constant Nusselt number and Sherwood number that vary only with the shape and the aspect ratio of the channel [35]. The Nusselt number and Sherwood number are assumed to be the same [36]. Therefore, the convective heat and mass transfer coefficients can be calculated using the following equations:

$$\alpha = \frac{Nu\lambda_a P}{4A} \tag{8}$$

$$K_y = \rho_a \frac{ShD_h P}{4A} \tag{9}$$

where D_h is the air diffusion coefficient, $m^2 \cdot s^{-1}$.

3.1.2. Boundary and initial conditions

The initial conditions were required as the simulation model is a transient model:

$$T_a(L,0) = T_0 \tag{10}$$

$$W(L,0) = 0 \tag{11}$$

$$T_w(L,0) = T_{w0} \tag{12}$$

$$\omega_a(L,0) = \omega_0 \tag{13}$$

During the dehumidification period, the boundary conditions are as follows:

$$T_a(0,\tau) = T_2 \tag{14}$$

$$\omega_a(0,\tau) = \omega_2 \tag{15}$$

The boundary conditions of the present model differ from those of the model used for open systems, because the regeneration air in open systems has a specific source. Specifically, in system A, the air after being dehumidified by the DW serves as the regeneration air, so the inlet parameter changes. Consequently, the regeneration air's humidity then becomes the same as the dehumidified air's humidity. In the regeneration period, the boundary conditions are as follows:

$$T(L,\tau) = T_4 \tag{16}$$

$$\omega(0,\tau) = \omega_4 \tag{17}$$

3.2. System performance indicators

The regeneration air flow ratio (γ), defined as the ratio of volume flow rates between the regeneration and process air, can be expressed as follows:

$$\gamma = \frac{q_{reg}}{q_{proc}} \times 100\% \tag{18}$$

where q_{reg} is the volume flow rate of the regeneration air, $m^3 \cdot h^{-1}$, and q_{proc} is the volume flow rate of the process air, $m^3 \cdot h^{-1}$.

D_{DW} represents the moisture removal amount of the DW and can be expressed as follows:

$$D_{DW} = (\omega_3 - \omega_2) \times 1000 \tag{19}$$

The moisture removal amount of the system (D_{tot}) can be calculated as follows:

$$\begin{aligned} D_{tot} &= [(\omega_1 - \omega_2) + (\omega_2 - \omega_3) \times (1 - \gamma)] \times 1000 \\ &= D_{DW} + D_{prec} + D_{cond} \end{aligned} \tag{20}$$

where D_{prec} is the moisture removal amount of the precooler and D_{cond} is the moisture removal amount of the condenser, respectively.

The improvement of the moisture removal capacity (ΔMRC), which was caused by the integration of DW, can be determined as follows:

$$\Delta MRC = \frac{(\omega_2 - \omega_3) \times (1 - \gamma)}{\omega_1} \times 100\% \tag{21}$$

The required amount of condensation of the system (Q_c) is the sum of both the one for pre-cooling process and condensation process and can be calculated as follows:

$$Q_c = Q_{c,prec} + Q_{c,cond} \tag{22}$$

where $Q_{c,prec}$ represents the cooling power of the precooling process, kW; and $Q_{c,cond}$ represents the cooling power of the condensation process, kW.

The energy consumption of the regeneration process (E_{reg}), can be calculated as:

$$E_{reg} = h_{reg} - h_{reg.o} \tag{23}$$

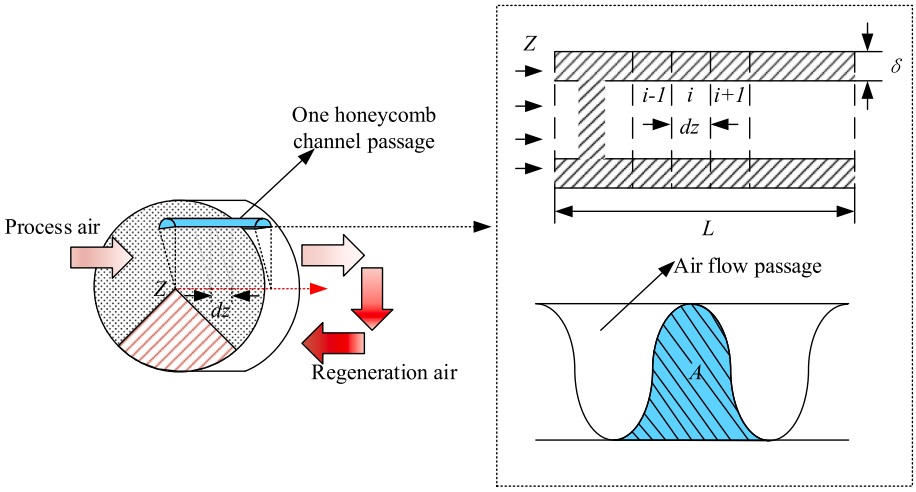

Fig. 3. Calculation domain of channel in desiccant wheel.

4. Results and discussion

4.1. Validation of simulation model

DW models are widely used in desiccant-based air conditioning systems to investigate and optimize system performance. These models need to be validated to ensure the accuracy and reliability of the obtained results. The DW model was verified by comparing the simulated and experimental results obtained from the literature survey [37]. The outlet air humidity of the DW was used for model validation. The input parameters are presented in Table 1. The air humidity variation overtime at the DW outlet is shown in Fig. 4. The maximum deviation between the experimental and simulated values was found to be approximately 8.3 %, indicating good agreement of the values calculated by the model. The system dehumidification capacity in the present work was compared with that reported in the literature, under the conditions of varying regeneration air temperature. The maximum deviation, observed to be only around 3.9 % compared with the results in Zhang's work [37], is noted in Fig. 5. Consequently, the simulation model is deemed appropriate for predicting the DW performance.

4.2. Comparison of different system configurations

The ambient conditions of the RRSD system are the actual operational conditions in the enclosed space [38]. A fixed ambient temperature of 40 °C was maintained, while the regeneration and pre-cooling temperatures were set at 150 °C and 20 °C, respectively. The process air volume flow rate was maintained at 200 $m^3\ h^{-1}$. To evaluate the efficacy of various system configurations, a theoretical approach was employed. The psychrometric chart of the three system configurations is depicted in Fig. 6.

The precooling process, represented by Lines 1 and 2, and the DW dehumidification process, represented by Lines 3 and 4, were consistent across all three systems, but the regeneration process differed. Although the regeneration air temperature and flow rate were identical across all configurations, the regeneration air humidity varied. The lowest regeneration air humidity appeared in system A.

4.2.1. Effect of ambient temperature

The thermal conditions within enclosed spaces are strongly dependent on the surrounding ambient temperature, which therefore is an important influencing factor. Variations in the ambient temperature induce consequential changes in both the system dehumidification capacity and the condensation capacity. The relationship between the system dehumidification capacity and two crucial factors—ambient temperature variations and system configurations—is depicted in Figs. 7 and 8. With increasing ambient temperature, the role of the pre-cooling process became more important for realizing a higher dehumidification rate (D_{tot}). The dehumidification performance of the system was found to be influenced by parameter γ. The optimal value of γ led to the highest dehumidification performance. Furthermore, as shown in Fig. 7(b), (c), and (d), the system with posterior diversion of the regeneration air (system A) exhibited the highest dehumidification performance owing to the low humidity of the regeneration air. Fig. 9 shows that system A exhibited the greatest increase in the dehumidification rate attributed to the increase in D_{DW}. The enhancement in ΔMRC is calculated as the ratio of the ΔMRC values observed under two distinct conditions to the smaller of these values. At the ambient temperature of 40 °C, D_{tot} and ΔMRC in system A were 3.7 % and 10.5 % higher, respectively, than those in system C. At lower ambient temperatures, the humidity of the regeneration air in system C decreased, realizing acceptable dehumidification performance. The results reveal that system A had better dehumidification performance at elevated ambient temperatures.

Figs. 9 and 10 depict the energy consumption variation of the system in response to changes in the ambient temperature and system configurations. Specifically, Fig. 9 (a) illustrates a pronounced reduction in the required condensation amount as the ambient temperature decreased. This was due to the reduction in the energy consumption required for pre-cooling with decreasing ambient temperature. In addition, Fig. 10 illustrates that the required condensation amount increased as the value of γ increased. This was because the regeneration air flow rate increased alongside γ, leading to an increase in the condensation amount required for the regeneration air cooling. As shown in Fig. 9 (b), when the ambient temperature reached 40 °C, the required condensation amount of system A was higher than that of system C, whereas when the ambient temperature dropped to 30 °C, the required condensation amount of system A was lower than that of system C. This was because the proportion of pre-cooling amount to total condensation amount was higher at higher ambient temperatures, and the required pre-cooling amount for system A was higher than that for system C, resulting in a higher required condensation amount. However, as the ambient temperature decreased, the effect of pre-cooling and condensation dehumidification decreased, and the dehumidification amount of system A was higher. Furthermore, the required amount of condensation for regeneration air was smaller, resulting in a decrease in the total condensation amount, which was smaller than that required for system C. Fig. 10 shows the required regeneration heat for the system as a function of the ambient temperature and γ. The process air temperature exerted no influence on the regeneration heat of both systems A and B. This intriguing observation can be explained based on the fact that the inlet temperature of

Table 1
Input parameters used for verification of model [37].

Parameter	Value	Parameter	Value
A	2.29 m^2	δ	0.15 mm
L	0.1 m	D_h	2.82×10^{-5} m^2 s^{-1}
L_v	2258 kJ kg^{-1}	K_y	3.5×10^{-7} $kg{\cdot}(m^2{\cdot}s)^{-1}$
c_{pm}	0.921 kJ (kg K) $^{-1}$	f_d	0.8 kg m^{-1}
V_{proc}	1.0 m s^{-1}	R	1.1
λ	1.98×10^{-4} kW·(m·K) $^{-1}$	W_{max}	0.4
t_{proc}	30 °C	ρ_d	790 kg m^{-3}
t_{reg}	70 °C	V_{reg}	1.3 m s^{-1}
φ_{proc}	85%RH		

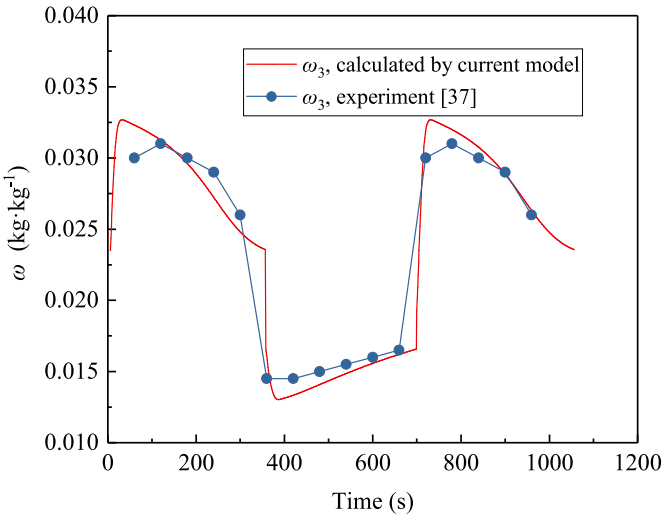

Fig. 4. Variations in specific humidity at DW outlet with time: Comparisons between simulation and experimental results.

the regeneration air in both systems, A and B, was solely influenced by the precooling process. As γ increased, the regeneration air flow rate increased, leading to a higher required regeneration heat. When the ambient temperature was 40 °C and γ reached the optimum value, the regeneration heat of system A was approximately 41 % lower than that of system C. In summary, system A exhibited a lower energy consumption and better dehumidification performance, with its superiority over the other systems being more obvious at higher ambient temperatures.

4.2.2. *Effect of ambient humidity*

The ambient humidity is known to be affected by occupants and equipment operation, and changes in indoor humidity have a substantial impact on the dehumidification performance and energy consumption of the system. Figs. 11 and 12 demonstrate how the system dehumidification performance varied with the ambient temperature and configuration. Pre-cooling became more important, as the increasing ambient temperature results in higher D_{tot} and lower ΔMRC. System A exhibited the best dehumidification performance because a lower humidity level and higher DW dehumidification performance were achieved by using the processed air as the regeneration air. At 90%RH, D_{tot} and ΔMRC in system A were 2.1 % and 42.8 % higher than those in system C, respectively. As the ambient humidity decreased, system C exhibited similar performance. In summary, at higher ambient humidity, the performance of system A was superior to that of the other two systems.

The required condensation capacity of the system decreased considerably as the ambient humidity decreased, as shown in Fig. 13. This was due to the decrease in the pre-cooling energy consumption with decreasing ambient humidity. Fig. 13 (b) shows that the required condensation capacity of system A was already lower than that of system C. This could be because at high ambient humidity, the ratio of pre-cooling amount to total condensation capacity in system A was higher than that in system C. Therefore, the total condensation capacity in system A was higher than that in system C. However, as the ambient humidity decreased, the ratio of the pre-cooling amount to the total condensation capacity in system A decreased, which resulted in a higher condensation amount for dehumidification, a lower one for regeneration, and thus a lower total condensation capacity compared with system C. The results show that system A exhibited a lower energy consumption and superior dehumidification performance, particularly at a high ambient humidity.

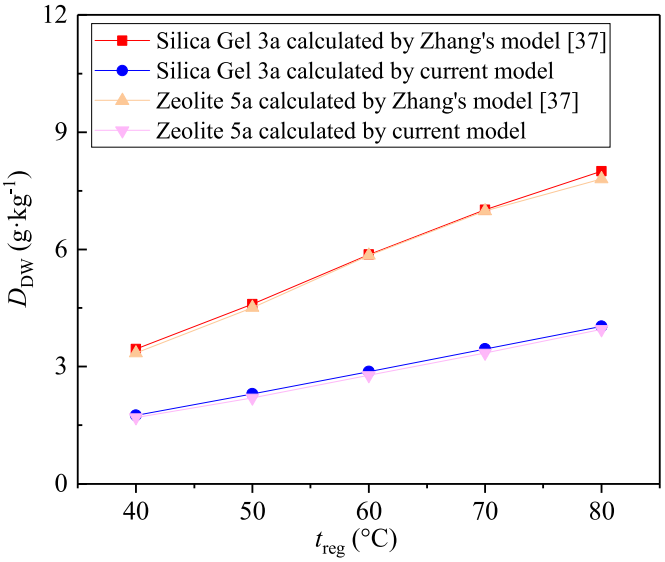

Fig. 5. Variations in D_{DW} with regeneration temperature.

4.2.3. *Effect of precooling temperature*

The system condensation temperature is a crucial factor that affects the dehumidification performance and energy consumption of the system, because it is limited by the energy storage amount and condensate water volume. Figs. 14 and 15 demonstrate how the dehumidification capacity of the system varies with γ at different precooling temperatures (t_{prec}). ΔMRC increased alongside γ under the same t_{prec} until the optimal value was reached. The optimal γ was determined by the highest D_{tot} achieved in the system. This was because increasing γ led to a larger regeneration air volume, which improved the dehumidification efficiency of the DW, thereby increased ΔMRC. Furthermore, the optimal γ increased slightly with the increase in t_{prec} due to the increase in the inlet air humidity of the DW caused by the rise in the condensing temperature, which resulted in a slight increase in the dehumidification capacity of the DW. As shown in Fig. 15 (b), the trend for ΔMRC changes is opposite to that for D_{tot} changes, and this was because of the decrease in the moisture removal amount of the condensation dehumidification. Under the simulated working conditions, the optimal γ was found to be between 30 % and 32 %, and the optimal ΔMRC was around 18.2 %.

Figs. 16 and 17 illustrate the variation in the system energy consumption with t_{prec} for the different system configurations. As shown in Fig. 16, the required condensation amount of the system reduced substantially with the increase in t_{prec}. This is due to the decrease in the energy consumption required for pre-cooling. Specifically, with every 1 °C rise in t_{prec}, the required condensation amount of the system decreased by 0.23 kW. Fig. 16 (b) reveals that when t_{prec} was 20 °C, system A required more condensation amount than system C, while at 24 °C, system A required less condensation amount than system C. However, as t_{prec} increased, the effect of pre-cooling and condensation dehumidification decreased, resulting in system A exhibiting a higher dehumidification capacity and lower condensation requirement for regeneration. This led to the total condensation amount being smaller

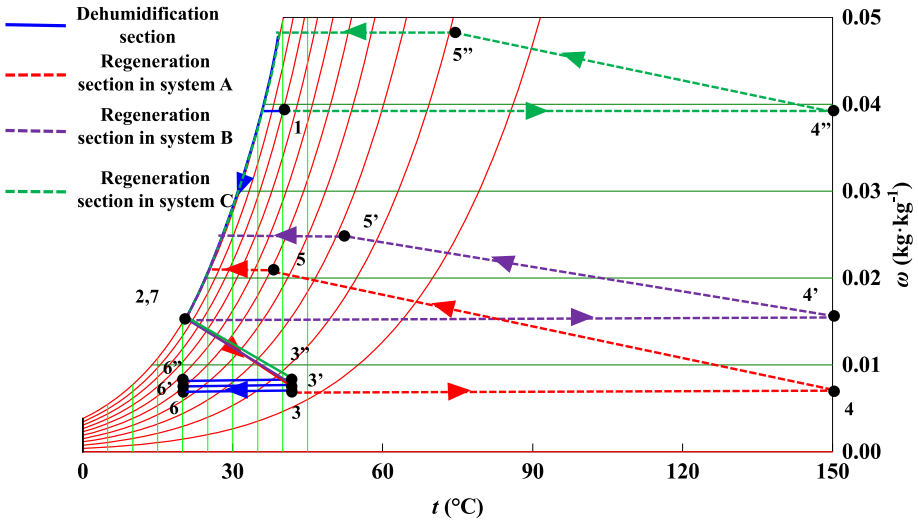

Fig. 6. Psychrometric processes for different system configurations.

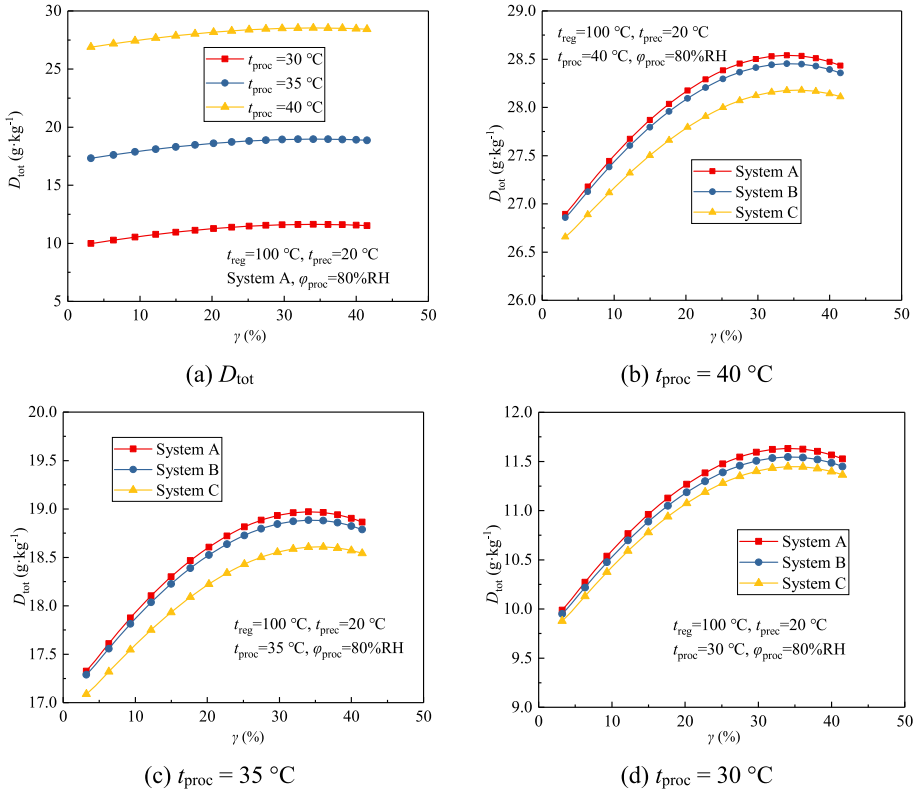

Fig. 7. Influence of T_{proc} and system configuration on D_{tot}.

than that of system C. Fig. 17 shows the variation in the required regeneration heat with t_{prec} and γ. As t_{prec} decreased, the required regeneration heat of the system slightly increased. This is because with decreasing temperature owing to the decrease in t_{prec}, the air required more regeneration heat after entering the regeneration heater. The system performed better with lower t_{prec}. Therefore, when adequate cooling sources are available, t_{prec} should be reduced as much as possible.

4.2.4. *Effect of regeneration air temperatures*

Fig. 18 depicts the impact of γ on the system dehumidification capacity at different regeneration air temperatures (t_{reg}) in system A. D_{tot} increased with increasing t_{reg} due to the improved dehumidification capacity of the DW when the regeneration temperature was high. Under simulated working conditions, the optimal γ ranged from 31 % to 35 %. Under the same t_{reg}, an increase in γ led to an increase in D_{tot}, and the extent of the increase in D_{tot} decreased with increasing t_{reg}. The possible explanation for this is that the dehumidification capacity of the DW increased with the rise in t_{reg}, as depicted in Fig. 10(a). In addition, when t_{reg} exceeded 130 °C, the improvement in DW dehumidification capacity was not substantial, and the rate of increase in D_{tot} reduced. At the regeneration temperatures of 80–150 °C, the optimal D_{tot} ranged from 27.4 to 29.3 g kg^{-1}, and the highest ΔMRC could be 13.0 % under simulated conditions.

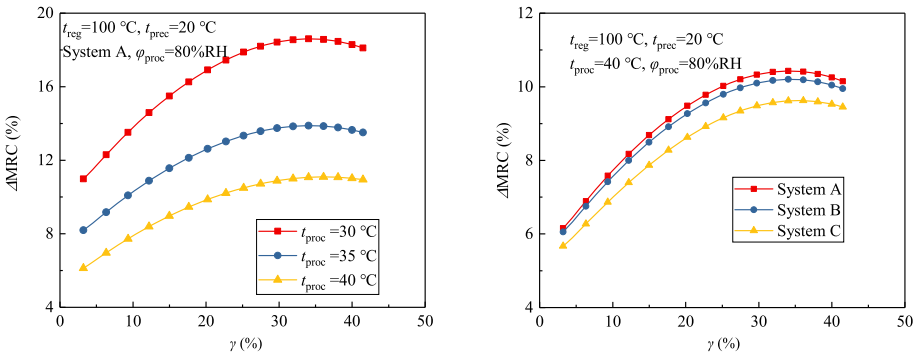

(a) ΔMRC (b) t_{proc} = 40 °C

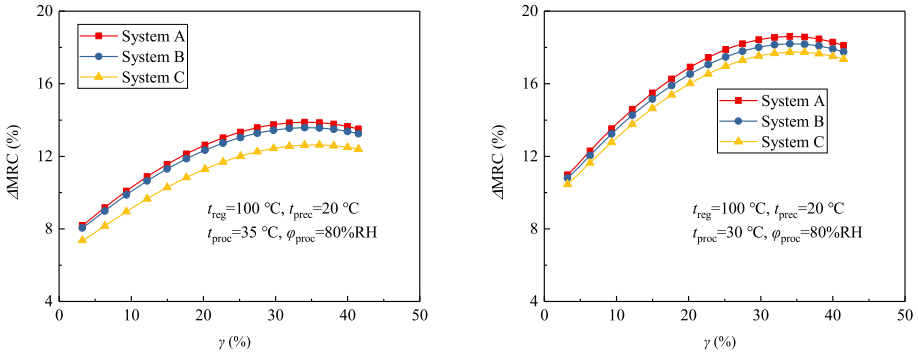

(c) t_{proc} = 35 °C (d) t_{proc} = 30 °C

Fig. 8. Influence of T_{proc} and system configuration on ΔMRC.

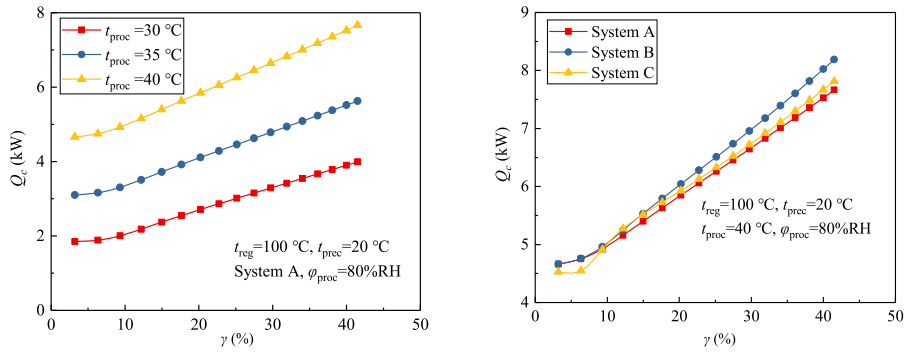

(a) Q_c (b) t_{proc} = 40 °C

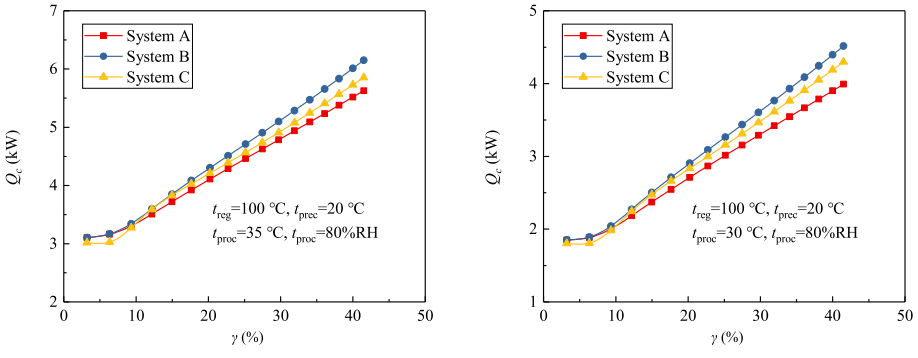

(c) t_{proc} = 35 °C (d) t_{proc} = 30 °C

Fig. 9. Influence of T_{proc} and system configuration on Q_c.

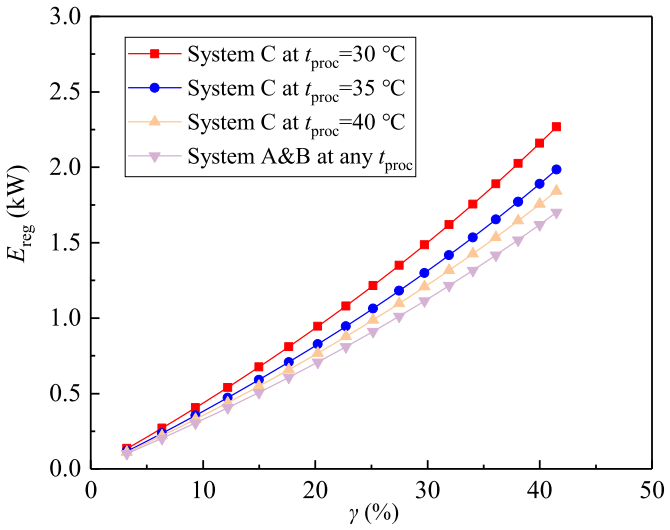

Fig. 10. Influence of T_{proc} and system configuration on E_{reg}.

From Fig. 19, it can be seen that Q_c and E_{reg} decreased with the increase in t_{reg}. The possible explanation for this is that when t_{reg} increased, the energy consumption for heating the regeneration air increased. Moreover, as shown in Fig. 19(b), the extent of the increase in the cooling power was influenced by the increase in the dehumidification capacity.

4.3. Comparison of different desiccant materials

The dehumidification capacity and energy consumption of six different desiccant materials were compared in the present work [37]. The thermodynamic properties of five different desiccants are shown in Table 2. There are distinct variations in particle size among various desiccant materials. Silica gel particles display a spherical morphology, while zeolite particles exhibit a square configuration, which further proves that there is diversity in their physical characteristics [39–41]. The experimental data of the synthesized metal silicate was obtained from previous work [9]. Fig. 20 presents the variations in the dehumidification performance of the system with different desiccant materials and γ in system A. The system with the synthesized metal silicate desiccant material exhibited the highest D_{tot} among all the systems. Fig. 20 (b) shows that the optimal ΔMRC could be improved by 34 % using synthesized metal silicate desiccant material instead of other materials. Synthesized metal silicate had a higher D_{tot} compared with other materials owing to its higher water adsorption capacity.

The energy consumption of the system with different desiccant materials is illustrated in Fig. 21. Notably, the system with the synthesized metal silicate had the lowest regeneration heat and condensation quantity requirements. However, the distinctions among the different materials were not substantial when the same operating parameters were used, and the energy consumption was solely dependent on the outlet temperature of the rotary wheel. The system with the synthesized metal silicate showed the highest dehumidification efficiency, with the lowest regeneration consumption and the minimum required amount of condensation.

4.3.1. Effect of maximum adsorption capacity

Sensitivity analysis is a powerful tool for investigating the impact of different parameters on the performance of a system. Different materials showcase distinct adsorption curves and capacities, and undertaking sensitivity analysis of these factors can effectively eliminate interferences, thereby facilitating the identification of the optimal material. In the present work, the impact of the DW material on the system dehumidification capacity and energy consumption was investigated. The maximum adsorption capacity (W_{max}) of the DW material was varied to examine its effect on the system performance.

The results shown in Fig. 22(a) indicate that the dehumidification capacity of the system increased with the rise in the W_{max} of the DW

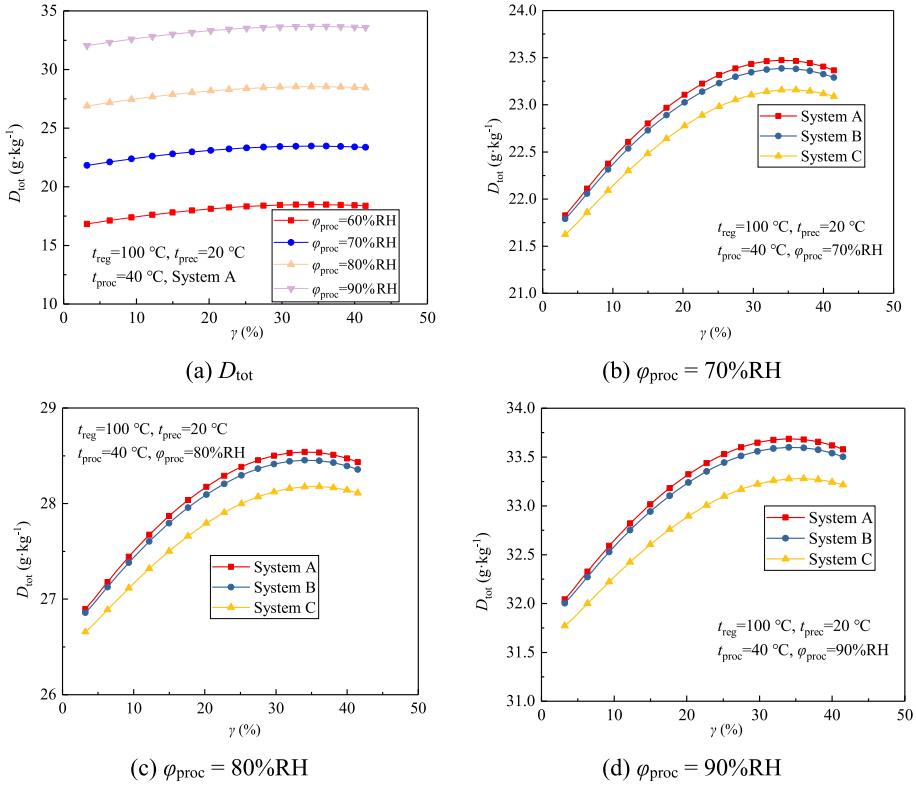

(a) D_{tot} (b) φ_{proc} = 70%RH

(c) φ_{proc} = 80%RH (d) φ_{proc} = 90%RH

Fig. 11. Influence of φ_{proc} and system configuration on D_{tot}.

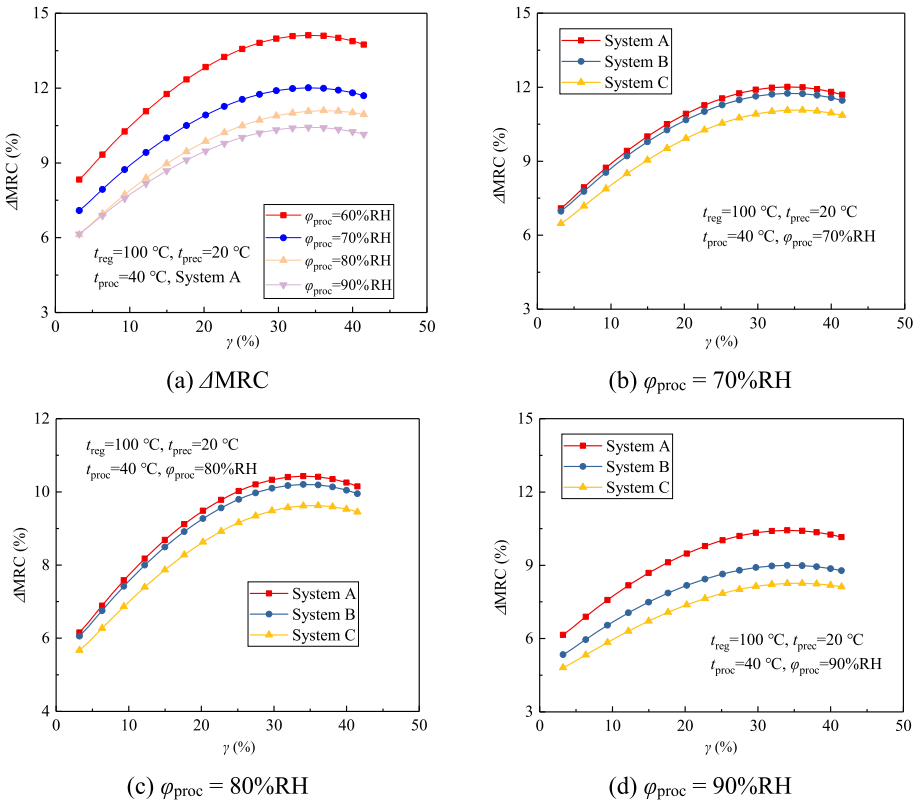

(a) ΔMRC (b) φ_{proc} = 70%RH

(c) φ_{proc} = 80%RH (d) φ_{proc} = 90%RH

Fig. 12. Influence of φ_{proc} and system configuration on ΔMRC.

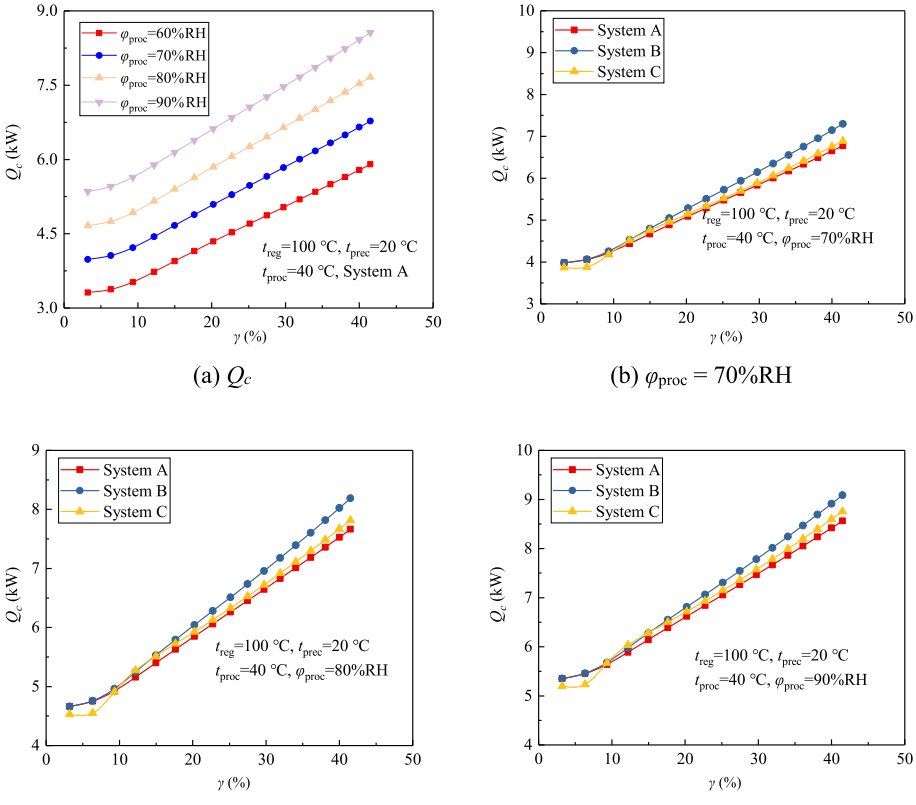

(a) Q_c (b) φ_{proc} = 70%RH

(c) φ_{proc} = 80%RH (d) φ_{proc} = 90%RH

Fig. 13. Influence of φ_{proc} and system configuration on Q_c.

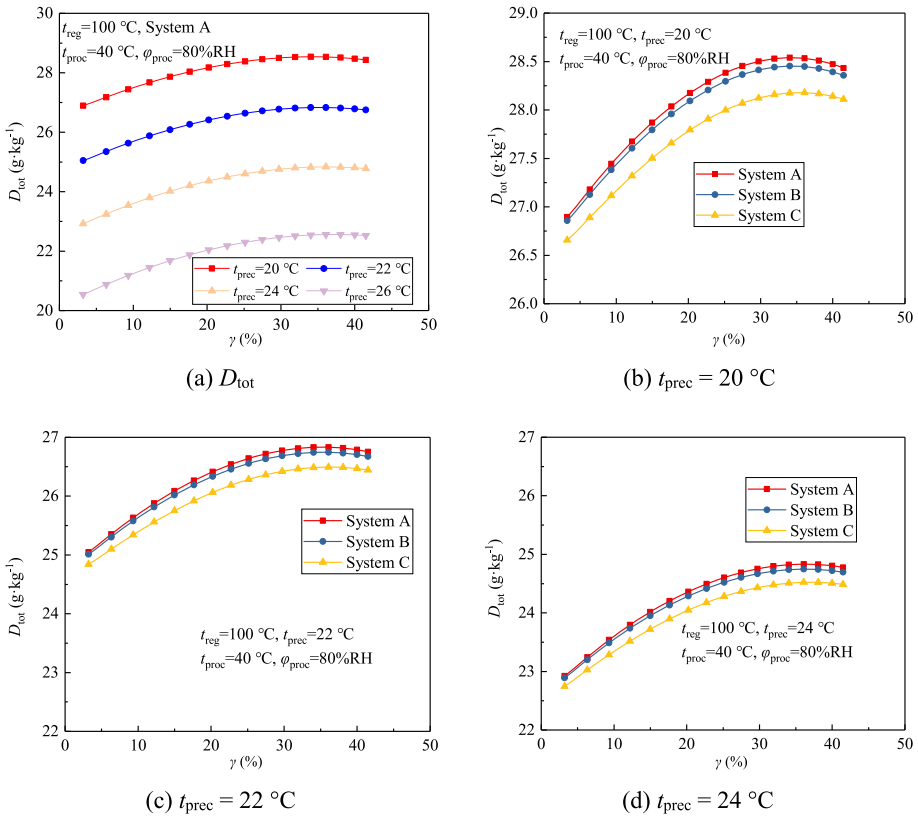

(a) D_{tot} (b) t_{prec} = 20 °C

(c) t_{prec} = 22 °C (d) t_{prec} = 24 °C

Fig. 14. Influence of t_{prec} and system configuration on D_{tot}.

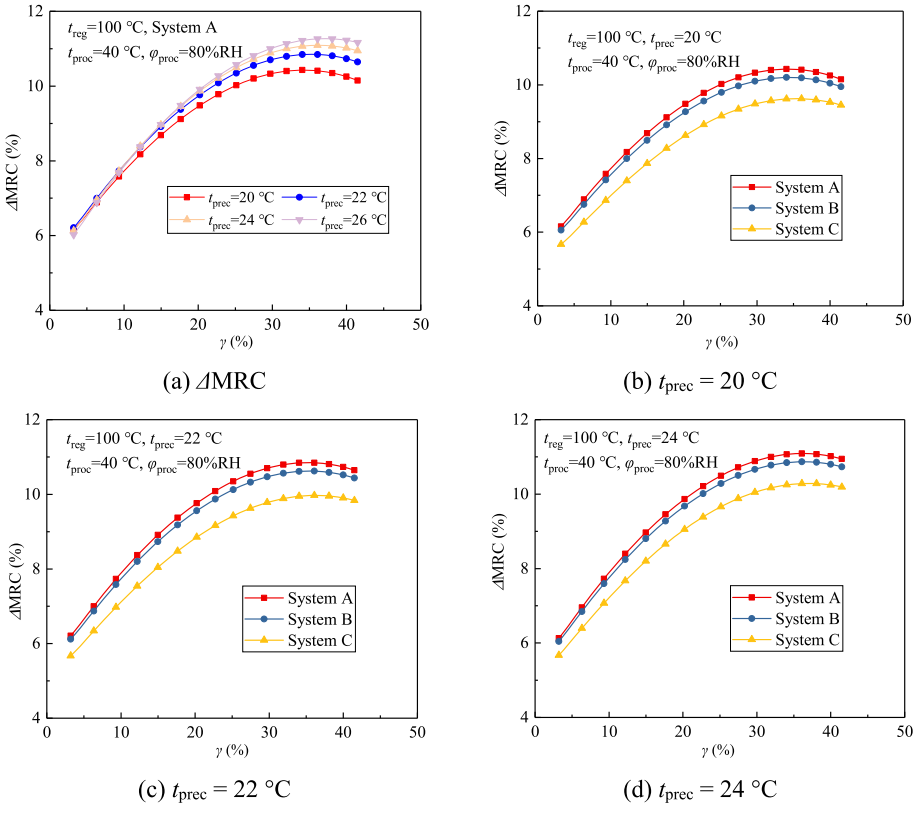

(a) ΔMRC (b) t_{prec} = 20 °C

(c) t_{prec} = 22 °C (d) t_{prec} = 24 °C

Fig. 15. Influence of t_{prec} and system configuration on ΔMRC.

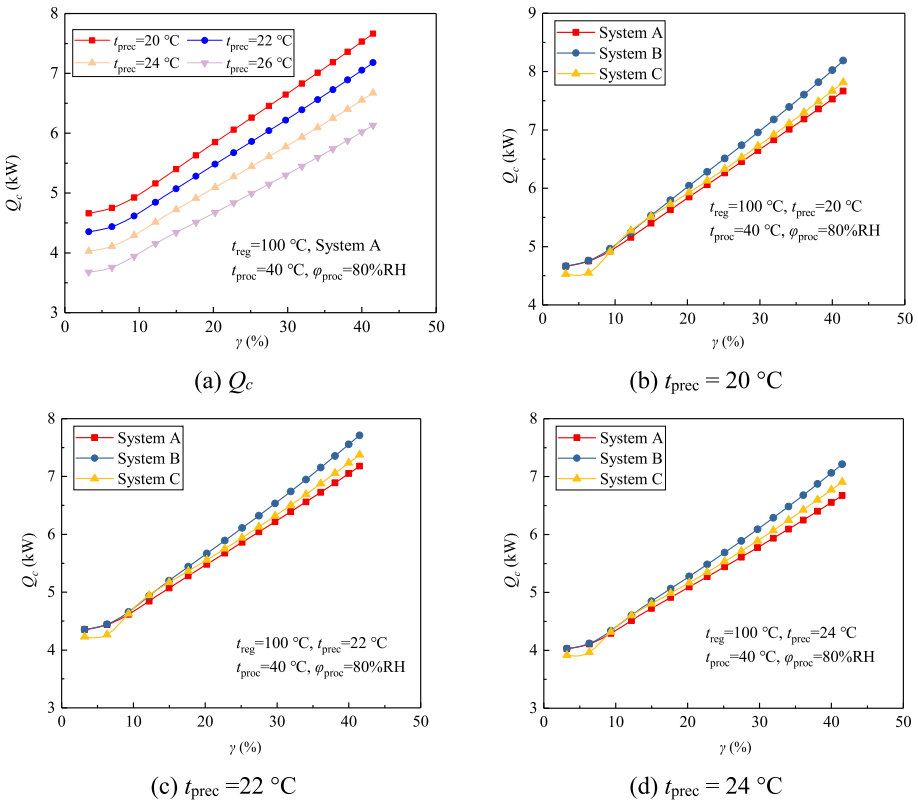

(a) Q_c (b) t_{prec} = 20 °C

(c) t_{prec} =22 °C (d) t_{prec} = 24 °C

Fig. 16. Influence of t_{prec} and system configuration on Q_c.

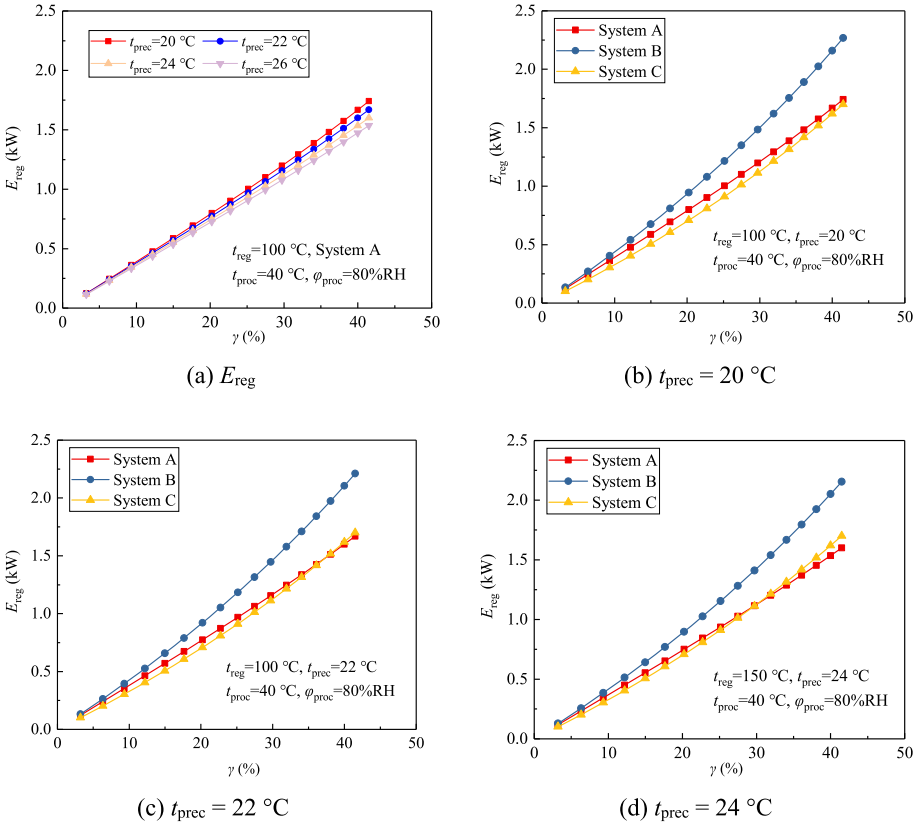

(a) E_{reg} (b) t_{prec} = 20 °C

(c) t_{prec} = 22 °C (d) t_{prec} = 24 °C

Fig. 17. Influence of t_{prec} and system configuration on E_{reg}.

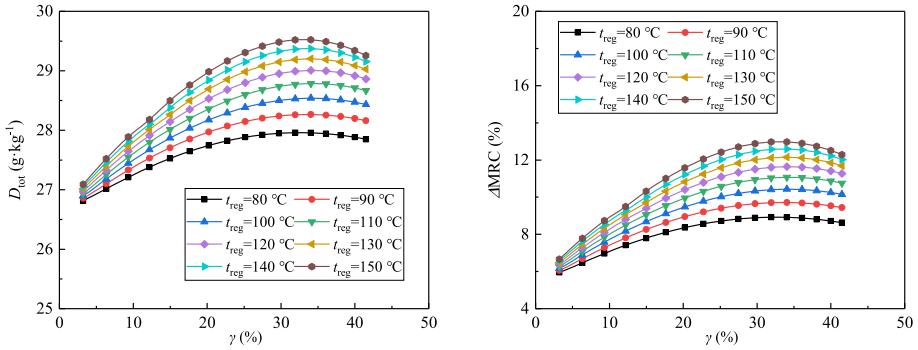

Fig. 18. Influence of t_{reg} on system dehumidification performance.

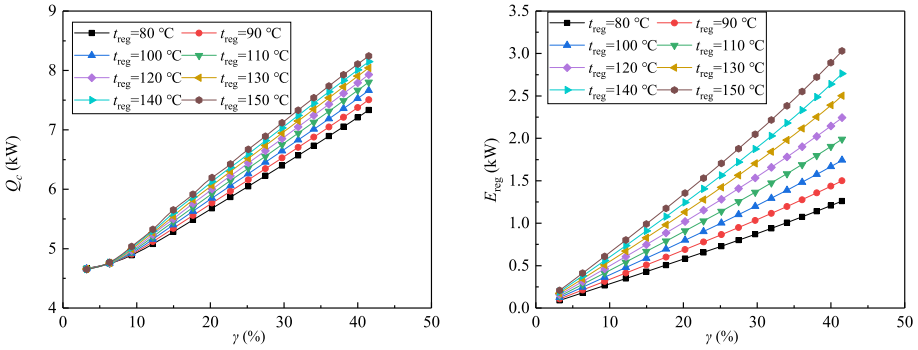

Fig. 19. Influence of t_{reg} on system energy performance.

material when γ was constant. The observed increase in the system dehumidification capacity can be attributed to the increasing D_{DW} corresponding to the increase in W_{max}. Notably, the optimal γ of the system gradually decreased with an increase in W_{max}. This was because the regeneration air flow rate required for maintaining a constant dehumidification rate was reduced after the dehumidification capacity of the DW was improved, resulting in decreasing energy consumption for DW regeneration. Based on the simulation results, the optimal γ was found to range from 27 % to 34 %.

Moreover, as shown in Fig. 23, the impact of W_{max} on system energy consumption was found to be minimal. This can be attributed to the fact that W_{max} primarily affected the dehumidification performance of the DW, as indicated by the observed changes in D_{tot} discussed earlier. Conversely, the cooling power and regeneration consumption of the system, which were closely related to the inlet and outlet air temperatures of the DW, were independent of W_{max}.

4.3.2. *Effect of separation factor*

Separation factor (R) is a crucial parameter affecting the absorption curve of the desiccant material. The increase in R, as shown in Fig. 24(a), was associated with the increase in D_{tot}. As R increased, the driving force for transferring the water vapor from the process air to the DW decreased, resulting in a decrease in the water vapor adsorption capacity of the DW. This led to a decrease in the dehumidification capacity of the system, and hence a decrease in D_{tot}.

According to Fig. 25(b), the R had almost no effect on the outlet air temperature of DW. A possible explanation for this is that the cooling power and regeneration consumption of the system were related to the inlet and outlet air temperatures of the DW. Therefore, R had no effect on the system energy consumption. Overall, the sensitivity analysis indicates that the DW material and its properties determine the system performance.

Table 2
Desiccant thermodynamic properties investigated in the present work.

Material	C_p/kJ·(kg·K)$^{-1}$	λ/W·(m·K)$^{-1}$	ρ/kg·m^{-3}	W_{max}	Q_{st}/kJ·kg^{-1}	R
Silica Gel B [37]	0.921	0.198	790	0.40	2362	1.1
Silica Gel 3A [42]	0.921	0.174	770	0.35	2380	1.1
Silica Gel RD [42]	0.921	0.198	800	0.37	2370	1.1
Silica Gel/LiCl [43]	0.921	0.239	875	0.60	2476	1.5
Zeolite 5A [37]	0.950	0.209	680	0.19	3974	0.2

5. Conclusions

The present work aimed to provide insights into the design and optimization of recirculated regenerative solid desiccant (RRSD) systems for dehumidifying enclosed spaces. Different setups of RRSD systems were investigated, with a focus on assessing their dehumidification capacity and energy efficiency. Simulation investigation was carried out to analyze the influence of external and internal factors on the system performance. The results highlight the importance of considering the diversion of regeneration air, selection of the appropriate desiccant materials, and optimization of operational parameters to achieve

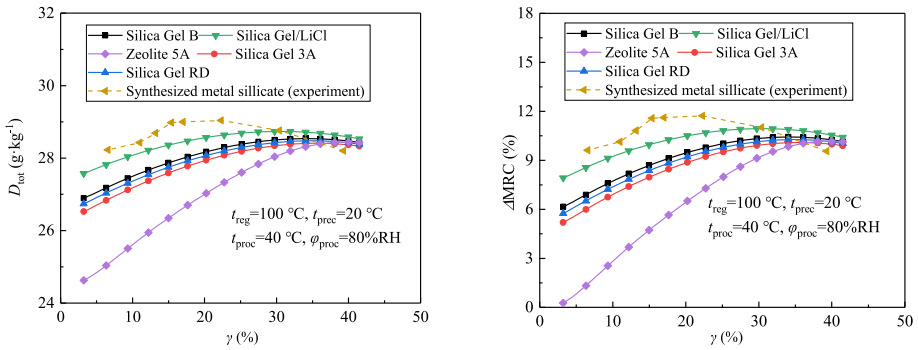

Fig. 20. Influence of different desiccant materials on system dehumidification performance.

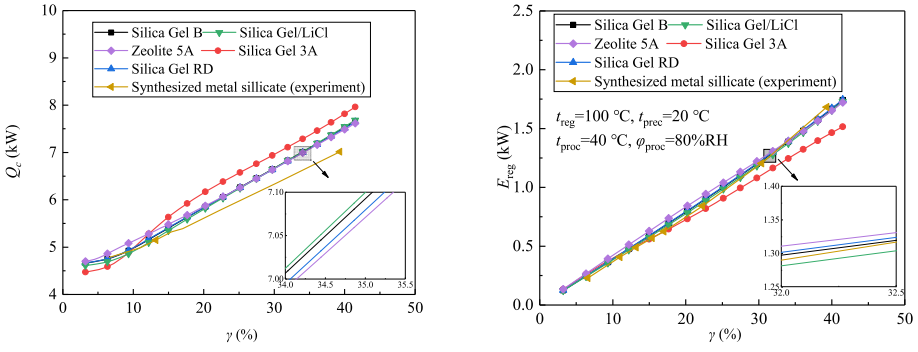

Fig. 21. Influence of different desiccant materials on system energy performance.

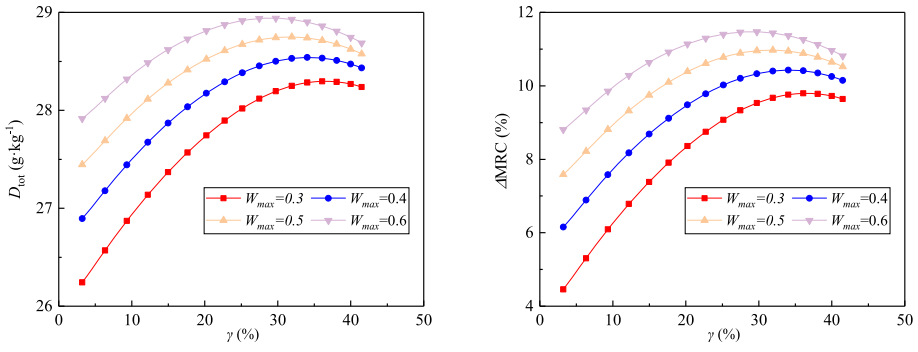

Fig. 22. Influence of w_{max} on system dehumidification performance.

improved system performance. The following conclusions can be drawn:

(1) The results show that the posterior diversion of regeneration air was preferable for RRSD system to improve the dehumidification performance. Among the three tested configurations, the regeneration air humidity was the lowest, and thus the dehumidification rate was the highest in system A. D_{tot} and ΔMRC of system A were 3.7 % and 42.8 % higher than those of system C, respectively. These findings emphasize the importance of considering regeneration air diversion in the RRSD system design, particularly in hot and humid environments.

(2) The energy consumption was reduced by the implementation of the posterior diversion regeneration. Energy consumption in system A was 13.3 % lower than that in system C. The utilization of the latent heat of the DW represents an important breakthrough in overcoming the limitations related to the excessive amount of air required for precooling. This result shows the flexibility of the system and contributes to sustainable dehumidification practices.

(3) The sensitivity analysis shows the pivotal role of the maximum adsorption capacity (W_{max}) as the most crucial internal factor influencing the system dehumidification capacity. This can be attributed to the notable enhancement in D_{DW}, which lead to the optimal value of γ decreasing with increasing W_{max}. Specifically, the range of optimal γ was determined to be approximately 23%–35 % under the specific simulation conditions in the present work. By contrast, the system energy performance is relatively insensitive to changes in these internal factors. The energy consumption (including E_{reg} and Q_c) was found to be largely independent of W_{max} and the separation factor.

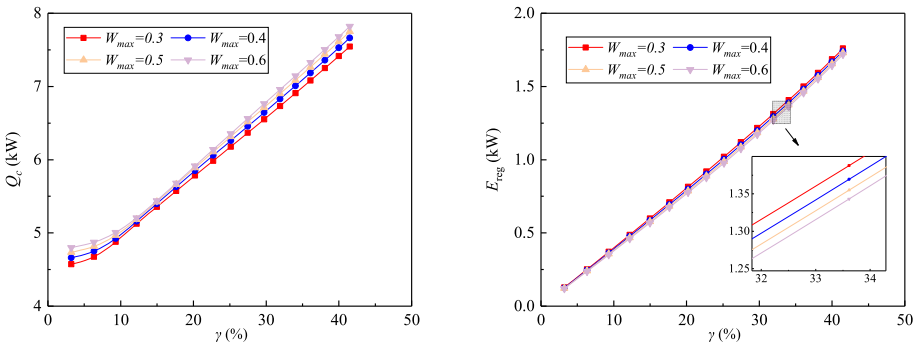

(a) Q_c (b) E_{reg}

Fig. 23. Influence of w_{max} on system energy performance.

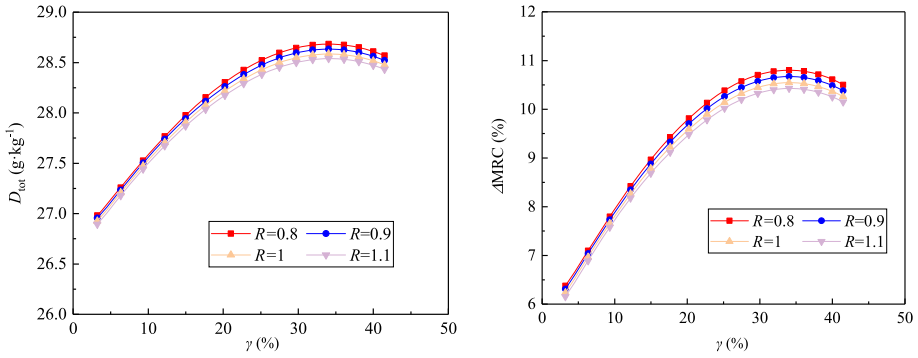

(a) D_{tot} (b) ΔMRC

Fig. 24. Influence of R on system dehumidification performance.

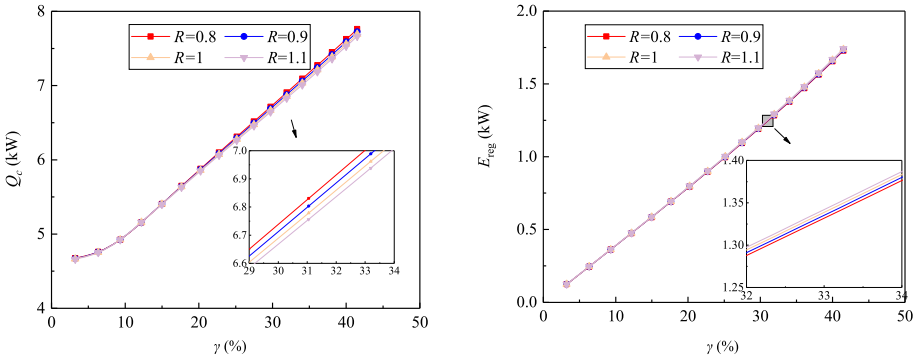

(a) Q_c (b) E_{reg}

Fig. 25. Influence of R on system energy performance.

Declaration of competing interest

The authors declare that they have no known competing financial interests or personal relationships that could have appeared to influence the work reported in this paper.

Data availability

The data that has been used is confidential.

Acknowledgments

This work was supported by the Natural Science Basic Research Plan in Shaanxi Province of China (No. 2023-JC-YB-444) and the Innovative Scientific Program of CNNC.

Nomenclature

Abbreviations

D	dehumidification rate, g·kg^{-1}
DW	desiccant wheel
GSR	gas side resistance
GSSR	gas and solid side resistance
ΔMRC	improvement of the moisture removal capacity, %
RH	relative humidity, %
rph	revolution per hour
RRSD	recirculated regenerative solid desiccant

Greek symbols

α	convective heat transfer coefficient, kW·(m^2·K) $^{-1}$
γ	regeneration air flow ratio, %

δ	half thickness of the desiccant wall, mm
λ	thermal conductivity, kW·(m·K) $^{-1}$
ρ	density, kg·m^{-3}
τ	time, s
φ	relative humidity, %RH
ω	humidity ratio, kg·kg^{-1}

Symbols

A	cross-section area of channel, m^2
c_p	specific heat capacity, J·(kg·K) $^{-1}$
D_h	air diffusion coefficient, m^2·s^{-1}
E_{reg}	regeneration heat, kW
f	mass per unit length in a single channel, kg·m^{-1}
h	specific enthalpy, kJ·kg^{-1}
L	length of the desiccant wheel, m
L_v	latent heat of vaporization, kJ·kg^{-1}
K_y	convective mass transfer coefficient, kg·(m^2·s) $^{-1}$
Nu	Nusselt number
P	perimeter of desiccant channel, m
P_{atm}	atmosphere pressure, Pa
P_{vs}	saturated vapor pressure, Pa
q	air flow rate, m^3·h^{-1}
Q_c	cooling power, kW
Q_{st}	absorption heat, J·kg^{-1}
R	separation factor
Sh	Sherwood number
T	temperature in Kelvin degree, K
t	temperature in Celsius degree, °C
V	velocity, m·s^{-1}
W	moisture in absorbent, kg·kg^{-1}
z	axial coordinated, m

Subscripts

a	air
d	desiccant
l	liquid water
m	matrix
w	desiccant wall
cond	condenser
o	outlet
prec	precooling
proc	process air
reg	regeneration air
tot	total

References

[1] Kaczorek D, Basinska M, Koczyk H. Hygrothermal behaviour of a room with different occupancy scenarios. J Build Eng 2023;66:105928.
[2] Hong S, Ge Y, Seo JK, Wang J, Liu P, Meng YS, et al. Wearable thermoelectrics for personalized thermoregulation. Sci Adv 2019;5:5.
[3] Tian S, Su X, Ge Y. Review on heat pump coupled desiccant wheel dehumidification and air conditioning systems in buildings. J Build Eng 2022;54:104655.
[4] Feng Y, Dai Y, Wang R, Ge T. Insights into desiccant-based internally-cooled dehumidification using porous sorbents: from a modeling viewpoint. Appl Energy 2022;311:188732.
[5] Wu X, Ge T, Dai Y, Wang R. Review on substrate of solid desiccant dehumidification system. Renew Sustain Energy Rev 2018;82:3236–49.
[6] Zhou X. Thermal and energy performance of a solar-driven desiccant cooling system using an internally cooled desiccant wheel in various climate conditions. Appl Therm Eng 2021;185:116077.
[7] Loubani ME, Ghadddar N, Ghali K, Itani M. Hybrid cooling system integrating PCM-desiccant dehumidification and personal evaporative cooling for hot and humid climates. Dry Technol 2021;33:101580.
[8] Song J, Sobhani B. Energy and exergy performance of an integrated desiccant cooling system with photovoltaic/thermal using phase change material and maisotsenko cooler. J Energy Storage 2020;32:101698.
[9] Su M, Han X, Chong D, Wang J, Liu J, Yan J. Experimental study on the performance of an improved dehumidification system integrated with precooling and recirculated regenerative rotary desiccant wheel. Appl Therm Eng 2021;199:117608.
[10] Saputra DA, Osaka Y, Tsujiguchi T, Haruki M, Kumita M, Kodama A. Experimental investigation of desiccant wheel dehumidification control method for changes in regeneration heat input. Energy 2020;205:118109.
[11] Asadi A, Roshanzadeh B. Improving performance of two-stage desiccant cooling system by analyzing different regeneration configurations. J Build Eng 2019;25:100807.
[12] Su M, Han X, Chang H, Chong D, Liu J, Yan J. Performance investigation and exergy analysis of a novel recirculated regenerative solid desiccant dehumidification system. J Build Eng 2023;67:106029.
[13] Ge F, Wang C. Exergy analysis of dehumidification systems: a comparison between the condensing dehumidification and the desiccant wheel dehumidification. Energy Convers Manag 2020;224:113343.
[14] Ding Z, Yu X, Ma Z, Wu W, Zhang L, Yu DW, Cheng HK. On-site measurement and simulation investigation on condensation dehumidification and desiccant dehumidification in Hong Kong. Energy Build 2022;254:111560.
[15] Aziz AN, Mahmoud S, Al-Dadah R, Ismail MA, Ai MK. Numerical and experimental investigation of desiccant cooling system using metal organic framework materials. Appl Therm Eng 2022;215:118940.
[16] Güzelel YE, Olmuş U, Çerçi KN, Büyükalaca O. New multiple regression and machine learning models of rotary desiccant wheel for unbalanced flow conditions. Int Commun Heat Mass 2022;134:106006.
[17] Ruivo CR, Angrisani G. The effectiveness method to predict the behaviour of a desiccant wheel: an attempt of experimental validation. Appl Therm Eng 2014;71:643–51.
[18] Na S, Chung Y, Kim MS. Performance analysis of an electric vehicle heat pump system with a desiccant dehumidifier. Energy Convers Manag 2021;236:114083.
[19] Wang N, Zhang J, Xia X. Desiccant wheel thermal performance modeling for indoor humidity optimal control. Appl Energy 2013;112:999–1005.
[20] Jani DB, Mishra M, Sahoo PK. Application of artificial neural network for predicting performance of solid desiccant cooling systems – a review. Renew Sustain Energy Rev 2017;80:352–66.
[21] Jani DB, Mishra M, Sahoo PK. Performance prediction of solid desiccant – vapor compression hybrid air-conditioning system using artificial neural network. Energy 2016;103:618–29.
[22] Motaghian S, Rayegan S, Pasdarshahri H, Ahmadi P, Rosen MA. Comprehensive performance assessment of a solid desiccant wheel using an artificial neural network approach. Int J Heat Mass Tran 2021;165:120657.
[23] Sahu PP, Swain A, Kanta SR. Modelling of desiccant wheels using radial basis neural networks. Mater Today Proc 2022;49:284–8.
[24] Chen X, Tu R, Li M, Yang X. Prediction models of air outlet states of desiccant wheels using multiple regression and artificial neural network methods based on criterion numbers. Appl Therm Eng 2022;204:117940.
[25] Zhu J, Chen W. A novel multivariate linear prediction model for the marine rotary desiccant air-conditioning by adding a dynamic correction factor. Appl Therm Eng 2015;78:101–9.
[26] Zendehboudi A. Implementation of GA-LSSVM modelling approach for estimating the performance of solid desiccant wheels. Energy Convers Manag 2016;127:245–55.
[27] Kang H, Choi S, Lee DY. Analytic solution to predict the outlet air states of a desiccant wheel with an arbitrary split ratio. Energy 2018;153:301–10.
[28] Guan B, Liu X, Wang X, Zhang T, Zhou Z. Regeneration energy analysis on desiccant wheel system in curling arena for the Winter Olympics. Build Environ 2022;214:108960.
[29] Pandelidis D, Pacak A, Cichoń A, Drąg P, Worek W, Cetin S. Numerical and experimental analysis of precooled desiccant system. Appl Therm Eng 2020;181:115929.
[30] Gao D, Sun Y, Ma Z, Ren H. A review on integration and design of desiccant air-conditioning systems for overall performance improvements. Renew Sustain Energy Rev 2021;141:110809.
[31] Dunkle RV. A method of solar air conditioning. Inst Mech Chem Eng Trans 1965;73:73–8.
[32] Jani DB, Mishra M, Sahoo PK. Investigations on effect of operational conditions on performance of solid desiccant based hybrid cooling system in hot and humid climate. Therm Sci Eng Prog 2018;7:76–86.
[33] Jani DB, Mishra M, Sahoo PK. Solid desiccant air conditioning – a state of the art review. Renew Sustain Energy Rev 2016;60:51–69.
[34] Chen L, Shi Q. Experimental study and performance analysis on a closed-cycle rotary dehumidification air conditioning system in deep underground spaces. Case Stud Therm Eng 2022;37:102245.
[35] Aprile M, Motta M. Grey-box modelling and in situ experimental identification of desiccant rotors. Appl Therm Eng 2013;51:55–64.
[36] Stefano DA, Kim DS. Effectiveness of a symmetric desiccant wheel operating in balanced flow condition: modeling and application. Int J Refrig 2018;88:347–59.
[37] Zhang L, Fu H, Yang Q, Xu J. Performance comparisons of honeycomb-type adsorbent beds (wheels) for air dehumidification with various desiccant wall materials. Energy 2014;65:430–40.
[38] Berglund LG, Yokota M, Potter AW. Thermo-physiological responses of sailors in a disabled submarine with interior cabin temperature and humidity slowly rising as

predicted by computer simulation techniques. 2013. Available at: https://apps.dtic.mil/sti/pdfs/ADA587308.pdf. [Accessed 30 May 2023].
[39] Wu Y, Li M, Wang X, Wang L. Fabrication and optical properties of photonic crystals of LiCl modified SiO2 colloidal spheres. In: Proceedings of 2016 International symposium on materials application and engineering (SMAE 2016). Engineering and Industry Technology Institute; 2016. p. 252–8.
[40] Rezk A, Al-Dadah R, Mahmoud S, Elsayed A. Characterisation of metal organic frameworks for adsorption cooling. Int J Heat Mass Tran 2012;55:7366–74.
[41] Liu J, Yang X, Wang C, Sun H. Synthesis of hierarchical 5A zeolites to improve the separation efficiency of n-paraffins. Adsorpt Sci Technol 2019;37:530–44.
[42] Ng KC, Chua HT, Chuang CY, Loke CH, Kashiwagi T, Akisawa A, et al. Experimental investigation of the silica gel–water adsorption isotherm characteristics. Appl Therm Eng 2001;21:1631–42.
[43] Jia C, Dai Y, Wu J, Wang R. Experimental comparison of two honeycombed desiccant wheels fabricated with silica gel and composite desiccant material. Energy Convers Manag 2006;47:2523–34.